Spectral weight transfer in strongly-correlated $Fe_{1.03}Te$

Y. M. Dai, A. Akrap,* J. Schneeloch, R. D. Zhong, T. S. Liu,† G. D. Gu, Q. Li, and C. C. Homes‡
Condensed Matter Physics and Materials Science Department,
Brookhaven National Laboratory, Upton, New York 11973, USA
(Dated: October 8, 2014)

The temperature dependence of the in-plane optical conductivity has been determined for $Fe_{1.03}Te$ above and below the magnetic and structural transition at $T_N \simeq 68$ K. The electron and hole pockets are treated as two separate electronic subsystems; a strong, broad Drude response that is largely temperature independent, and a much weaker, narrow Drude response with a strong temperature dependence. Spectral weight is transferred from high to low frequency below T_N, resulting in the dramatic increase of both the low-frequency conductivity and the related plasma frequency. The change in the plasma frequency is due to an increase in the carrier concentration resulting from the closing of the pseudogap on the electron pocket, as well as the likely decrease of the effective mass in the antiferromagnetic state.

PACS numbers: 72.15.-v, 75.50.Bb, 78.30.-j

arXiv:1406.4166v2 [cond-mat.str-el] 7 Oct 2014

The discovery of superconductivity at high temperatures in the iron-arsenic materials [1–3] prompted the search for this phenomenon in other iron-based systems, including the iron-chalocogenide materials. FeSe is an ambient-pressure superconductor with a critical temperature $T_c \simeq 8$ K; while the partial substitution of Te for Se almost doubles the T_c, the end compound FeTe is not a superconductor [4]. For nearly stoichiometric $Fe_{1+\delta}Te$ there is a first-order structural and magnetic transition [5–7] from a tetragonal, paramagnetic (PM) state to a monoclinic, antiferromagnetic (AFM) state at $T_N \simeq 68$ K. In the low-temperature phase a bond-order wave is observed that has been attributed to ferro-orbital ordering [8]. At ambient pressure, the structural and magnetic properties depend strongly on the amount of excess Fe [9, 10]. $Fe_{1+\delta}Te$ is a poor metal that exhibits a non-metallic resistivity that increases with decreasing temperature [11–13]; at T_N the resistivity drops discontinuously, followed by a metallic response decreasing steadily with temperature. Optical works on $Fe_{1+\delta}Te$ observe a rapid increase in the low-frequency optical conductivity below T_N that has been attributed to a reduction of the free-carrier scattering rate [11, 12]. Electronic structure calculations reveal the multiband nature of this material with three hole-like bands at the center of the Brillouin zone and two electron-like bands at the corners [14]; this result is in agreement with Hall-effect measurements in $Fe_{1+\delta}Te$ where both the electron and hole carriers are observed [15]. Angle-resolved photoemission spectroscopy (ARPES) is able to observe some of the predicted bands, but they are strongly renormalized with a large mass enhancement $m^*/m_b \approx 6-20$, suggesting a strongly-correlated metal [16–20]. The enhancement of the effective mass in the PM state has been attributed to an orbital blocking mechanism [21]. In addition, a pseudogap of $\simeq 65$ meV has been observed on the electron pocket in the PM state that closes in the AFM state [22]. The multiband nature of this material suggests that an analysis of the optical data that considers two different types of free-carrier contributions is in order [23].

In this Letter we report on the detailed temperature dependence of the in-plane optical conductivity of $Fe_{1.03}Te$ above and below T_N where the electron and hole pockets have been treated as two separate electronic subsystems. We infer that the hole pocket has a large scattering rate, resulting in an almost incoherent response that is largely temperature independent. This is in contrast to the low-frequency conductivity associated with the electron pocket, which while roughly constant above T_N, increases anomalously at low temperature. This behavior is accompanied by a transfer of spectral weight over much of the mid-infrared region to low energy. The striking increase in the low-frequency conductivity is due to a dramatic increase in the plasma frequency associated with the electron pocket below T_N, suggesting that we are observing the closing of the pseudogap with a commensurate increase in the carrier concentration, as well as a possible reduction in the effective mass.

Single crystals with good cleavage planes (001) were grown by a unidirectional solidification method with a nominal composition of $Fe_{1.03}Te$ and a magnetic and structural transition at $T_N = 68$ K. The reflectance from the cleaved surface of a mm-sized single crystal has been measured at a near-normal angle of incidence for several temperatures above and below T_N over a wide frequency range ($\sim$ 2 meV to 4 eV) for light polarized in the *a*-*b* planes using an *in situ* overcoating technique [24]. The temperature dependence of the reflectance of $Fe_{1.03}Te$ is shown in Fig. 1(a) in the far-infrared region and at higher energies in Fig. 1(b). Above T_N the reflectance is metallic but shows relatively little temperature dependence; however, below T_N the reflectance increases rapidly in this region. This behavior is consistent with the resistivity (shown in the inset) which increases slightly from room temperature to just above T_N, but which decreases rapidly below T_N. In order to understand the metallic

Typeset by REVTEX

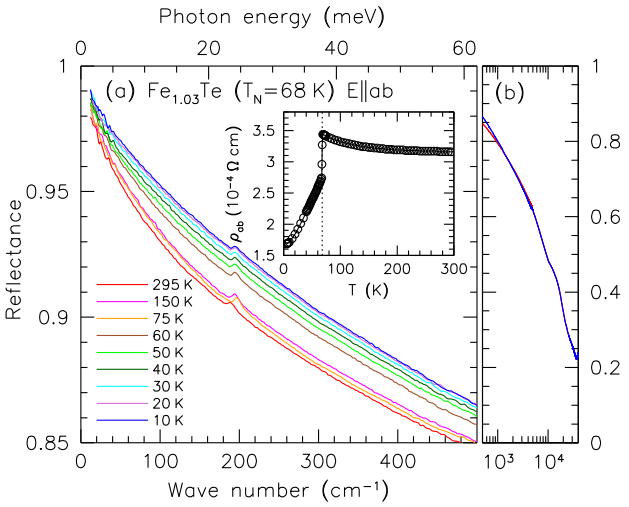

FIG. 1. (a) The reflectance of $Fe_{1.03}Te$ in the far-infrared region for light polarized in the Fe-Te planes at several temperatures above and below T_N. Inset: The temperature dependence of the in-plane resistivity. (b) The high-frequency reflectance at 295 and 5 K.

behavior of this material below T_N, the complex conductivity has been determined from a Kramers-Kronig analysis of the reflectance [25], which requires the reflectance to be determined over the entire frequency interval. Given the conducting nature of this material, the Hagen-Rubens form for the reflectance is used in the $\omega \rightarrow 0$ limit, $R(\omega) = 1 - a\sqrt{\omega}$, where a is chosen to match the data at the lowest-measured frequency point. Above the highest-measured frequency the reflectance is assumed to be constant up to 7.5×10^4 cm^{-1}, above which a free electron gas asymptotic reflectance extrapolation $R(\omega) \propto 1/\omega^4$ is assumed [26].

The real part of the in-plane optical conductivity is shown in Fig. 2 for several temperatures above and below T_N. The conductivity is difficult to explain within a simple Drude model, which would follow a $\sigma_1(\omega) = \sigma_0/(1+\omega^2\tau^2)$ form, where $\sigma_0 = \sigma_1(\omega \rightarrow 0)$ and $1/\tau$ is the free-carrier scattering rate. Above T_N the conductivity is essentially frequency and temperature independent over much of the infrared region; only the region below $\simeq$ 100 cm^{-1} shows any indication of following a Drude-like response. Below T_N there is a small but abrupt decrease in the conductivity over much of the mid-infrared region at the same time that the Drude-like component increases dramatically in strength, indicating a transfer of spectral weight from high to low frequency. The spectral weight is defined as the area under the conductivity curve over a given interval $N(\omega_c, T) = \int_0^{\omega_c} \sigma_1(\omega, T)\, d\omega$. The temperature dependence of the normalized spectral weight for different cut-off frequencies is shown in Fig. 3. For small cut-off frequencies the spectral weight is roughly constant for $T > T_N$; however, for $T < T_N$ it increase quickly. As the cut-off frequency is increased this behavior becomes less pronounced until by $\omega_c \simeq 4000$ cm^{-1} the spectral weight of the free carriers has been completely captured and a temperature dependence is no longer observed. A redistribution of spectral weight below T_N has also been observed in ARPES [18, 22].

In a single-band material, the evolution of a low-frequency Drude response to an incoherent mid-infrared band may be explained in one of two ways. First, the Drude response may be superimposed on interband transitions, modeled as Lorentz oscillators, that begin at very low frequency; while there is evidence for transitions at energies as low as 30 meV in the iron-based materials [27, 28], this is still not low enough to reproduce incoherent component observed in this material. A second approach is to assume a strongly-renormalized scattering rate due to electronic correlations [29]. However, $Fe_{1+\delta}Te$ is a multiband material [14], negating the application of the single-band model to this material. For simplicity, the multiple hole and electron bands are gathered into single electron and hole pockets that are treated as two separate electronic subsystems using the so-called two-Drude model [23] with the complex dielectric function

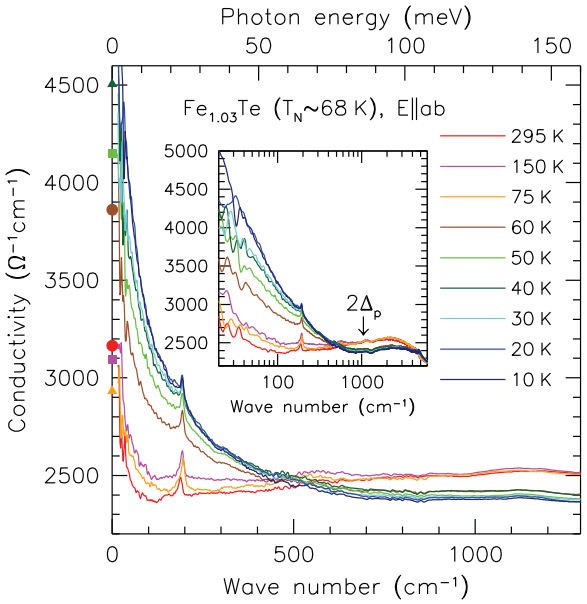

FIG. 2. The temperature dependence of the real part of the optical conductivity of $Fe_{1.03}Te$ for light polarized in the a-b planes above and below T_N (the origin for the y axis is offset). The symbols denote the values for the dc conductivity obtained from transport measurements. Inset: The temperature dependence of the optical conductivity shown over a larger energy scale showing the transfer of spectral weight from high to low energy below T_N. The arrow indicates the energy scale in the optical conductivity for the pseudogap on the electron pocket in the PM state.

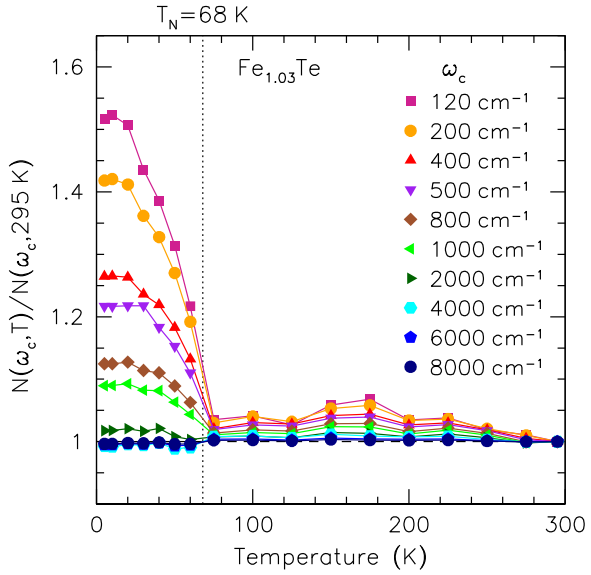

FIG. 3. The temperature dependence of the normalized spectral weight as a function of cut-off frequency, ω_c. For values of $\omega_c \gtrsim 4000$ cm^{-1} the spectral weight is completely captured and no temperature dependence is observed.

$$\tilde{\epsilon} = \epsilon_1 + i\epsilon_2,$$

$$\tilde{\epsilon}(\omega) = \epsilon_\infty - \sum_{j=1}^{2} \frac{\omega_{p,D;j}^2}{\omega^2 + i\omega/\tau_{D,j}} + \sum_k \frac{\Omega_k^2}{\omega_k^2 - \omega^2 - i\omega\gamma_k}, \quad (1)$$

where ϵ_∞ is the real part of the dielectric function at high frequency. In the first sum $\omega_{p,D;j}^2 = 4\pi n_j e^2/m_j^*$ and $1/\tau_{D,j}$ are the square of the plasma frequency and scattering rate for the delocalized (Drude) carriers in the jth band, respectively, and n_j and m_j^* are the carrier concentration and effective mass. In the second summation, ω_k, γ_k and Ω_k are the position, width, and strength of the kth vibration or bound excitation. The complex conductivity is $\tilde{\sigma}(\omega) = \sigma_1 + i\sigma_2 = -i\omega[\tilde{\epsilon}(\omega) - \epsilon_\infty]/60$ (in units of Ω^{-1}cm^{-1}). The fits to the optical conductivity using this approach are in general quite good and reveal a strong, broad Drude component in combination with a narrow, much weaker Drude component; in addition, there are several strong, overdamped Lorentzian oscillators in the mid- and near-infrared regions. Below T_N there is a suppression of the optical conductivity over much of the mid-infrared region and a transfer of spectral weight from high to low energy. This result is in agreement with previous optical work [12], and is similar to what is observed in the normal state of the superconducting iron-arsenic material $Ba_{0.6}K_{0.4}Fe_2As_2$ [30]. The strong Lorentzian oscillator centered in the mid infrared shifts to a somewhat higher frequency below T_N, but its strength does not vary and it broadens only slightly. The results of the fits at several temperatures above and below T_N are summarized in Table I.

We infer from the observation of the hole-like band determined from scattering interference and the virtual absence of the electron band in a related material [31], Hall effect [15] and the calculated band structure [32], that the broad, temperature-independent Drude component is associated with the hole pockets, and that the narrow, strongly temperature-dependent component is associated with the electron pockets.

TABLE I. The temperature dependence of the Drude parameters for the electron and hole pockets and the Lorentz oscillators (bound excitations); the estimated uncertainties are for the fitted parameters is approximately 5%. All units are in cm^{-1} unless otherwise indicated.

T (K)	$\omega_{p,D;1}$	$1/\tau_{D,1}$	$1/\tau_{D,2}^a$	$\omega_{L,1}^b$	$\gamma_{L,1}^b$
295	1010	~ 28	805	3030	12 110
150	1200	~ 38	776	3004	12 016
100	1180	~ 40	780	3027	12 001
75	1050	~ 38	786	3023	12 022
60	1850	~ 48	788	3285	12 391
50	2035	~ 48	765	3305	12 470
40	2300	~ 48	774	3278	12 399
30	2570	~ 48	784	3335	12 462
20	2820	~ 48	782	3342	12 473
10	3010	~ 48	772	3350	12 505

[a] $T > T_N$, $\omega_{p,D;2} = 10\,700$; $T < T_N$, $\omega_{p,D;2} = 11\,200$ cm^{-1}.
[b] $\Omega_{L,1} = 40\,800$ cm^{-1}.

Although the optical conductivity is nearly frequency independent over much of the infrared region and displays little temperature dependence after entering the PM state, there is a dramatic increase in the low-frequency optical conductivity below T_N. To isolate this behavior, the contributions of the broad Drude term and the Lorentzian oscillators (Table I) have been removed, resulting in a residual component which we infer is due to the contribution to the optical conductivity from the electron pocket,

$$\sigma_{1,D;1} = \sigma_1 - \sigma_{1,D;2} - \sum_j \sigma_{1,L;j}. \quad (2)$$

The resulting series of curves, shown in Fig. 4, have a Drude-like response. Using the contribution to the conductivity from the broad Drude term, $\sigma_{D2} = \omega_{p,D;2}^2 \tau_{D,2}/60$, and the values determined from transport, $\sigma_{dc} = 1/\rho_{ab}$, the dc conductivity values for the electron pocket should be $\sigma_{1,D;1}(\omega \to 0) = \sigma_{dc} - \sigma_{D2}$; these symbols are shown at the origin of Fig. 4. In the zero-frequency limit the conductivity extrapolates to these values reasonably well. The Drude fits to the narrow component have been constrained to agree with these values and indicate that while $\omega_{p,D;1}$ is increasing rapidly below T_N, the scattering rate $1/\tau_{D,1}$ is roughly constant. In fact, given that the Drude profile is a Lorentzian centered at zero frequency and the width at half maximum is the scattering rate, the fact that $1/\tau_{D,1}$ is not changing may be observed simply by inspection (dotted line in

Fig. 4). The two dashed lines in Fig. 4 show the results of the fits just above T_N and for $T \ll T_N$; in general the fits close to T_N are quite good while for $T \ll T_N$ the fits are somewhat poorer, perhaps because there are in fact two electron pockets rather than just one we have used to model the low-frequency conductivity.

The rapid increase of the low-frequency conductivity below T_N is striking. Normally, this behavior is associated with a decrease in the scattering rate, resulting in a narrowing of the Drude feature. While this narrowing results in the transfer of spectral weight from high to low frequency, the total weight associated with the individual Drude component should remain constant. However, not only does the scattering rate actually increase slightly upon entering the AFM state (whereupon it remains roughly constant below T_N), the spectral weight is observed to increase dramatically, indicating that is in fact the plasma frequency that is increasing. The temperature dependence of $\omega^2_{p,D;1}$ below T_N shown in the inset of Fig. 4 follows a mean-field temperature dependence. Given the definition of $\omega^2_{p,D;1} = 4\pi n_1 e^2/m^*_1$, then either the carrier concentration is increasing or the effective mass is decreasing. However, in this instance there is evidence to suggest that both quantities are changing below T_N.

In the PM state there is a partial gap (pseudogap) on the electron pocket of $\Delta_p \simeq 65$ meV (525 cm^{-1})

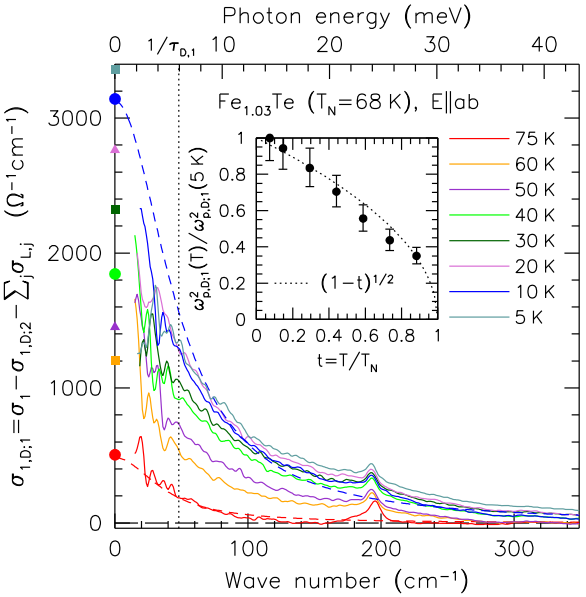

FIG. 4. The low-frequency in-plane optical conductivity of $Fe_{1.03}Te$ with the broad Drude contribution and the Lorentz oscillators removed. The symbols at the origin denote $\sigma_{dc} - \sigma_{D2}$ (see text). The dotted line denotes $1/\tau_{D,1} = 6$ meV, while the dashed lines are Drude fits at 75 and 10 K using the values from Table I. Inset: The square of the normalized plasma frequency for the narrow Drude component versus the reduced temperature; the dotted line denotes mean-field behavior.

[22]. In the optical conductivity a pseudogap in the spectrum of excitations shifts spectral weight associated with the free-carriers in the electron pocket to energies above $2\Delta_p \simeq 130$ meV (1050 cm^{-1}) resulting in a localized, incoherent response. This is precisely what is observed in Fig. 3, where $\omega_c > 2\Delta_p$ is necessary to recover the full spectral weight. However, below T_N the pseudogap is observed to close [22] resulting in coherent charge transport; this is consistent with the appearance of quasiparticles below T_N [18]. As a result, the number of carriers in the electron pocket (n_1) will increase below T_N with a commensurate increase in the plasma frequency, ($\omega_{p,D;1}$). In addition, there is also evidence that in the PM state of FeTe there is a large mass enhancement of the Fe d_{xy} orbital of $m^*/m_{band} \simeq 7$; this effect is attributed to an orbital-blocking mechanism [21]. In the AFM state the spin fluctuations are observed to decrease [18] and most signs of correlations disappear [22], suggesting that orbital blocking, and as a consequence the effective mass, may be reduced below T_N. Thus, the increase in n_1 and the decrease in m^*_1 may combine in tandem to lead to an increase of the plasma frequency for the carriers on the electron pocket in the AFM state.

To conclude, we have measured the in-plane optical properties of $Fe_{1.03}Te$ above and below T_N. The optical conductivity has been described using the two-Drude model, revealing a strong component with a large scattering rate associated with the hole pocket that varies little with temperature, and a weaker component with a much smaller scattering rate associated with the electron pocket that displays a strong temperature dependence below T_N. The plasma frequency associated with the carriers in the electron pocket increases anomalously below T_N due to an increase in the carrier concentration following the closing of the pseudogap, as well as the possible decrease of the effective mass in the AFM state.

The authors thank J. C. Davis, K. Haule, J. Hwang, G. Kotliar, J. H. Shim, and I. Zaliznyak for helpful discussions. Research supported by the U.S. Department of Energy (DOE), Office of Basic Energy Sciences, Division of Materials Sciences and Engineering under Contract No. DE-AC02-98CH10886. RDZ and JS were supported by the Center for Emergent Superconductivity, an Energy Frontier Research Center, DOE.

* Present address: University of Geneva, CH-1211 Geneva 4, Switzerland
† School of Chemical Engineering and Environment, North University of China, Taiyuan, Shanxi PRC 030051
‡ homes@bnl.gov

[1] Y. Kamihara, T. Watanabe, M. Hirano, and H. Hosono, J. Am. Chem. Soc. **130**, 3296 (2008).
[2] Z.-A. Ren, J. Yang, W. Lu, W. Yi, X.-L. Shen, Z.-C. Li, G.-C. Che, X.-L. Dong, L.-L. Sun, F. Zhou, and Z.-X.

Zhao, EPL **82**, 57002 (2008).
[3] D. C. Johnston, Adv. Phys. **59**, 803 (2010).
[4] R. Khasanov, M. Bendele, A. Amato, P. Babkevich, A. T. Boothroyd, A. Cervellino, K. Conder, S. N. Gvasaliya, H. Keller, H.-H. Klauss, H. Luetkens, V. Pomjakushin, E. Pomjakushina, and B. Roessli, Phys. Rev. B **80**, 140511(R) (2009).
[5] W. Bao, Y. Qiu, Q. Huang, M. A. Green, P. Zajdel, M. R. Fitzsimmons, M. Zhernenkov, S. Chang, M. Fang, B. Qian, E. K. Vehstedt, J. Yang, H. M. Pham, L. Spinu, and Z. Q. Mao, Phys. Rev. Lett. **102**, 247001 (2009).
[6] I. A. Zaliznyak, Z. Xu, J. M. Tranquada, G. Gu, A. M. Tsvelik, and M. B. Stone, Phys. Rev. Lett. **107**, 216403 (2011).
[7] I. A. Zaliznyak, Z. J. Xu, J. S. Wen, J. M. Tranquada, G. D. Gu, V. Solovyov, V. N. Glazkov, A. I. Zheludev, V. O. Garlea, and M. B. Stone, Phys. Rev. B **85**, 085105 (2012).
[8] D. Fobes, I. A. Zaliznyak, Z. Xu, R. Zhong, G. Gu, J. M. Tranquada, L. Harriger, D. Singh, V. O. Garlea, M. Lumsden, and B. Winn, Phys. Rev. Lett. **112**, 187202 (2014).
[9] X. Liu, C.-C. Lee, Z. J. Xu, J. S. Wen, G. Gu, W. Ku, J. M. Tranquada, and J. P. Hill, Phys. Rev. B **83**, 184523 (2011).
[10] E. E. Rodriguez, C. Stock, P. Zajdel, K. L. Krycka, C. F. Majkrzak, P. Zavalij, and M. A. Green, Phys. Rev. B **84**, 064403 (2011).
[11] G. F. Chen, Z. G. Chen, J. Dong, W. Z. Hu, G. Li, X. D. Zhang, P. Zheng, J. L. Luo, and N. L. Wang, Phys. Rev. B **79**, 140509 (2009).
[12] J. N. Hancock, S. I. Mirzaei, J. Gillett, S. E. Sebastian, J. Teyssier, R. Viennois, E. Giannini, and D. van der Marel, Phys. Rev. B **82**, 014523 (2010).
[13] J. Jiang, C. He, Y. Zhang, M. Xu, Q. Q. Ge, Z. R. Ye, F. Chen, B. P. Xie, and D. L. Feng, Phys. Rev. B **88**, 115130 (2013).
[14] A. Subedi, L. Zhang, D. J. Singh, and M. H. Du, Phys. Rev. B **78**, 134514 (2008).
[15] I. Tsukada, M. Hanawa, S. Komiya, A. Ichinose, T. Akike, Y. Imai, and A. Maeda, Physica C: Superconductivity **471**, 625 (2011), the 23rd International Symposium on Superconductivity.
[16] Y. Xia, D. Qian, L. Wray, D. Hsieh, G. F. Chen, J. L. Luo, N. L. Wang, and M. Z. Hasan, Phys. Rev. Lett. **103**, 037002 (2009).
[17] A. Tamai, A. Y. Ganin, E. Rozbicki, J. Bacsa, W. Meevasana, P. D. C. King, M. Caffio, R. Schaub, S. Margadonna, K. Prassides, M. J. Rosseinsky, and F. Baumberger, Phys. Rev. Lett. **104**, 097002 (2010).
[18] Y. Zhang, F. Chen, C. He, L. X. Yang, B. P. Xie, Y. L. Xie, X. H. Chen, M. Fang, M. Arita, K. Shimada, H. Namatame, M. Taniguchi, J. P. Hu, and D. L. Feng, Phys. Rev. B **82**, 165113 (2010).
[19] Z. K. Liu, R.-H. He, D. H. Lu, M. Yi, Y. L. Chen, M. Hashimoto, R. G. Moore, S.-K. Mo, E. A. Nowadnick, J. Hu, T. J. Liu, Z. Q. Mao, T. P. Devereaux, Z. Hussain, and Z.-X. Shen, Phys. Rev. Lett. **110**, 037003 (2013).
[20] M. M. Qazilbash, J. J. Hamlin, R. E. Baumbach, L. Zhang, D. J. Singh, M. B. Maple, and D. N. Basov, Nat. Phys. **5**, 647 (2009).
[21] Z. P. Yin, K. Haule, and G. Kotliar, Nat. Mater. **10**, 932 (2011).
[22] P.-H. Lin, Y. Texier, A. Taleb-Ibrahimi, P. Le Fèvre, F. Bertran, E. Giannini, M. Grioni, and V. Brouet, Phys. Rev. Lett. **111**, 217002 (2013).
[23] D. Wu, N. Barišić, P. Kallina, A. Faridian, B. Gorshunov, N. Drichko, L. J. Li, X. Lin, G. H. Cao, Z. A. Xu, N. L. Wang, and M. Dressel, Phys. Rev. B **81**, 100512(R) (2010).
[24] C. C. Homes, M. Reedyk, D. A. Crandles, and T. Timusk, Appl. Opt. **32**, 2976 (1993).
[25] M. Dressel and G. Grüner, *Electrodynamics of Solids* (Cambridge University Press, Cambridge, 2001).
[26] F. Wooten, *Optical Properties of Solids* (Academic Press, New York, 1972) pp. 244–250.
[27] P. Marsik, C. N. Wang, M. Rössle, M. Yazdi-Rizi, R. Schuster, K. W. Kim, A. Dubroka, D. Munzar, T. Wolf, X. H. Chen, and C. Bernhard, Phys. Rev. B **88**, 180508 (2013).
[28] B. Valenzuela, M. J. Calderón, G. León, and E. Bascones, Phys. Rev. B **87**, 075136 (2013).
[29] J. W. Allen and J. C. Mikkelsen, Phys. Rev. B **15**, 2952 (1977).
[30] Y. M. Dai, B. Xu, B. Shen, H. Xiao, H. H. Wen, X. G. Qiu, C. C. Homes, and R. P. S. M. Lobo, Phys. Rev. Lett. **111**, 117001 (2013).
[31] M. P. Allan, A. W. Rost, A. P. Mackenzie, Y. Xie, J. C. Davis, K. Kihou, C. H. Lee, A. Iyo, H. Eisaki, and T.-M. Chuang, Science **336**, 563 (2012).
[32] D. J. Singh and M.-H. Du, Phys. Rev. Lett. **100**, 237003 (2008).